

## Article

# Fixed Yellow-to-Blue Intensity Ratio of Dy<sup>3+</sup> in KY(CO<sub>3</sub>)<sub>2</sub> Host for Emission Color Tuning

Lei Huang<sup>1</sup>, Jian Qian<sup>1</sup>, Shijian Sun<sup>1</sup> and Dechuan Li<sup>1,2,\*</sup>

<sup>1</sup> School of Physics and Electronic Information, Huaibei Normal University, Huaibei 235000, China; hbnun991210@163.com (L.H.); qianjianwyyx@163.com (J.Q.); sunsj\_0105@163.com (S.S.)

<sup>2</sup> Anhui Province Key Laboratory of Pollutant Sensitive Materials and Environmental Remediation, Huaibei 235000, China

\* Correspondence: lidechuan@chnu.edu.cn

**Abstract:** Dy<sup>3+</sup>, Ce<sup>3+</sup> co-doped KY(CO<sub>3</sub>)<sub>2</sub> phosphors with a monoclinic structure were synthesized using the hydrothermal method to create a fixed yellow-to-blue ratio emission. The [YO<sub>8</sub>] polyhedron, consisting of a Y atom and eight oxygen atoms, forms a relatively independent microstructure within the KY(CO<sub>3</sub>)<sub>2</sub> host. Y<sup>3+</sup> ions are partially replaced by Ce<sup>3+</sup> or Dy<sup>3+</sup> ions to construct the [CeO<sub>8</sub>] or [DyO<sub>8</sub>] polyhedral fluorescence emission unit. The spectral measurements indicate that Ce<sup>3+</sup> and Dy<sup>3+</sup> can maintain relatively independent fluorescence emission characteristics in the KY(CO<sub>3</sub>)<sub>2</sub> host. The yellow-to-blue intensity ratio of Dy<sup>3+</sup> remains close to 1 and does not change with the variation in the doping concentration of KY(CO<sub>3</sub>)<sub>2</sub>:Dy<sup>3+</sup> and KY(CO<sub>3</sub>)<sub>2</sub>:Dy<sup>3+</sup>,Ce<sup>3+</sup> phosphors. When Ce<sup>3+</sup> and Dy<sup>3+</sup> are co-doped with KY(CO<sub>3</sub>)<sub>2</sub>, the emission intensities of Dy<sup>3+</sup> under 339 nm and 365 nm excitation increase by 8.43 and 2.32 times, respectively, through resonance energy transfer and cross-relaxation. All Ce<sup>3+</sup>-doped KY(CO<sub>3</sub>)<sub>2</sub>:Dy<sup>3+</sup> phosphors can emit white light. Among them, the emitted light of KY(CO<sub>3</sub>)<sub>2</sub>:3%Dy<sup>3+</sup>,5%Ce<sup>3+</sup> is closest to standard daylight. Therefore, a stable [YO<sub>8</sub>] polyhedral structure can be used to achieve more color tuning of light.

**Keywords:** Dy<sup>3+</sup>; color tuning; intensity ratio; phosphors



**Citation:** Huang, L.; Qian, J.; Sun, S.; Li, D. Fixed Yellow-to-Blue Intensity Ratio of Dy<sup>3+</sup> in KY(CO<sub>3</sub>)<sub>2</sub> Host for Emission Color Tuning. *Materials* **2024**, *17*, 1438. <https://doi.org/10.3390/ma17061438>

Academic Editor: Heesun Yang

Received: 19 February 2024

Revised: 18 March 2024

Accepted: 19 March 2024

Published: 21 March 2024



**Copyright:** © 2024 by the authors. Licensee MDPI, Basel, Switzerland. This article is an open access article distributed under the terms and conditions of the Creative Commons Attribution (CC BY) license (<https://creativecommons.org/licenses/by/4.0/>).

## 1. Introduction

Dy<sup>3+</sup> is an important rare earth luminescent ion with strong blue and yellow emission [1,2]. Tunable emission properties are widely used in the fields of solid-state lighting [3–5], temperature sensing [6–8], gamma detection [9], and anti-counterfeiting [10,11]. The intense emission of two visible lights is attributed to the energy level transitions from <sup>4</sup>F<sub>9/2</sub> to <sup>6</sup>H<sub>15/2</sub> and <sup>6</sup>H<sub>13/2</sub> [3]. The <sup>4</sup>F<sub>9/2</sub> → <sup>6</sup>H<sub>15/2</sub> transition belongs to the magnetic dipole transition, whereas the <sup>4</sup>F<sub>9/2</sub> → <sup>6</sup>H<sub>13/2</sub> transition belongs to the hypersensitive electric dipole transition, which is greatly affected by the crystal field environment [12]. The electric field environment around Dy<sup>3+</sup> can be modified by doping with different concentrations of ions in the host. The higher the asymmetry is, the greater the yellow emission intensity [13,14]. An asymmetric crystal field changes the yellow-to-blue intensity ratio in the Dy<sup>3+</sup> emission spectrum, resulting in an unpredictable variety of luminescent color. However, the doping concentration should not be excessive for Dy<sup>3+</sup>. An excessive concentration in the crystal lattice could reduce the distance between two Dy<sup>3+</sup> ions and promote cross-relaxation and resonance energy transfer [14,15]. Consequently, the emission intensity is weakened due to concentration quenching [16–18]. Therefore, it is essential to investigate an asymmetric fluorescent material with a relatively fixed intensity ratio for intense emission [19].

Asymmetric microstructures are widely used for the emission of Dy<sup>3+</sup> [20,21]. A phosphor with a tetragon tungsten bronze structure is used to produce stable blue and yellow light emissions [12]. However, the yellow/blue ratio is limited due to the relatively balanced tendency of Dy<sup>3+</sup> in both pentagonal-A and square-B sites of the PbTa<sub>2</sub>O<sub>6</sub> crystal

structure. The yellow emission of  ${}^4F_{9/2} \rightarrow {}^6H_{13/2}$  corresponds to an electric dipole transition, which is sensitive to the asymmetric arrangement of  $Dy^{3+}$ . The degree of asymmetry in the  $Dy^{3+}$  environment is often described by the yellow-to-blue intensity ratio (Y/B) [19]. The yellow light intensity is highly uncertain in differently doped hosts. The Y/B ratios are larger than 1 in  $Dy^{3+}$ -doped  $Bi_2MoO_6$  [15],  $K_3YB_6O_{12}$  [16], and  $YGdPO_4$  [20] and less than 1 in  $Y_4Al_2O_9$  [5],  $PbTa_2O_6$  [12], and  $YAl_5O_{12}$  [22]. Moreover, the value of Y/B does not change synchronously with the concentration of  $Dy^{3+}$  [23]. Variation in the Y/B value in the  $Dy^{3+}$  emission spectrum may induce uncertainty in the luminescence color. Therefore, a stable crystal field environment with high emission intensity is particularly important for the single luminescent color of  $Dy^{3+}$ . A host with a polyhedral structure is one of the good options.

As one of the fluorescent crystals, the monoclinic  $KY(CO_3)_2$  is a good optical material with high optical transmittance [24]. In the  $[Y(CO_3)_2]^-$  framework of the  $KY(CO_3)_2$  host,  $Y^{3+}$  is coordinated to eight  $O^{2-}$  to form a relatively independent  $[YO_8]$  polyhedron. The  $Y^{3+}$  in this polyhedron can be replaced by other rare earth ions to achieve a stable luminescent emission [25]. The radius of  $Dy^{3+}$  ions is close to  $Y^{3+}$ . The independent crystal field environment in the  $[DyO_8]$  polyhedron ensures stable emission of  $Dy^{3+}$  in yellow and blue light, which means that the light color in  $KY(CO_3)_2:Dy^{3+}$  is relatively stable. In this work,  $Dy^{3+}$  and  $Ce^{3+}$  co-doped  $KY(CO_3)_2$  are prepared, and the structures, morphologies, luminescence, decay curves, and color tuning are discussed.

## 2. Materials and Methods

A series of  $KY_{1-x-y}(CO_3)_2:x\%Dy^{3+},y\%Ce^{3+}$  ( $KYC:x\%Dy^{3+},y\%Ce^{3+}$ ) phosphors were prepared by the hydrothermal method. High-purity  $Y(NO_3)_3 \cdot H_2O$  (99.99%),  $Dy(NO_3)_3 \cdot H_2O$  (99.99%), and  $Ce(NO_3)_3 \cdot H_2O$  (99.99%) were used as raw materials for the chemical reactions (Shanghai Xianding Biotechnology Co., Ltd., Shanghai, China). The detailed synthesis process has been described in the literature [25]. First, all rare earth nitrates were weighed according to the stoichiometric ratio and dissolved in 5 mL deionized water. Second, the nitrate solution was added dropwise into a vigorously stirred 25 mL  $K_2CO_3$  solution (0.55 mol/L). Third, the pH value of the nitrate mixed solution was adjusted to 9.5 using dilute nitric acid. After 30 min of vigorous stirring, the mixed solution was transferred to a 50 mL reactor and heated to 200 °C for 12 h. The reaction precipitate was filtered and washed with deionized water, and the final fluorescent powder was obtained.

The crystal structures of  $KYC:x\%Dy^{3+},y\%Ce^{3+}$  were characterized with an X-ray diffractometer. Lattice parameters were fitted by Rietveld refinement using FullProf software (5.10). The morphologies of grains and the types of elements were analyzed with cold-field emission scanning electron microscopy (Regulus 8220, Hitachi High-Tech Co., Tokyo, Japan). The luminescent properties of  $KYC:x\%Dy^{3+},y\%Ce^{3+}$  were detected with an FLS920 fluorescence spectrophotometer equipped with a 450 W Xe-lamp (Edinburgh Instruments, Livingston, UK). The decay curves were recorded with a 60 W microsecond flashlamp (Edinburgh Instruments, Livingston, UK).

## 3. Results and Discussion

### 3.1. Crystal Structures

Figure 1a shows the XRD patterns of  $KYC:3\%Dy^{3+},5\%Ce^{3+}$ ,  $KYC:5\%Ce^{3+}$ , and  $KYC:3\%Dy^{3+}$ . Three diffraction spectra of the sample show the similar diffraction peaks with slight differences in intensities. All diffraction peaks match well with the standard diffraction spectrum of  $KHo(CO_3)_2$  (JCPDS: 1-88-1419). No secondary phases are detected in the spectrum. The crystal structure is the same as reported in the literature [24]. In the enlarged image,  $2\theta$  angles at the (002) crystal plane are observed to shift to a lower angle in comparison to  $KHo(CO_3)_2$ . The reason for lattice expansion is that the radius of doped ions is larger than that of  $Ho^{3+}$  ions. The ionic radii of  $Ho^{3+}$ ,  $Y^{3+}$ ,  $Dy^{3+}$ , and  $Ce^{3+}$  are 1.015, 1.019, 1.027, and 1.143 Å [26], respectively. Figure 1b presents the Rietveld refinement of  $KYC:3\%Dy^{3+},5\%Ce^{3+}$  with FullProf software.  $KHo(CO_3)_2$  was selected as

the initial structural mode. The refined cell parameters are presented in Table 1. From the refined lattice parameters of KYC:3%Dy<sup>3+</sup>,5%Ce<sup>3+</sup>, the values of the cell volume and parameters are larger than those of KY(CO<sub>3</sub>)<sub>2</sub>, which indicates that Ce<sup>3+</sup> and Dy<sup>3+</sup> ions were successfully doped into the monoclinic structure of KY(CO<sub>3</sub>)<sub>2</sub> [27].

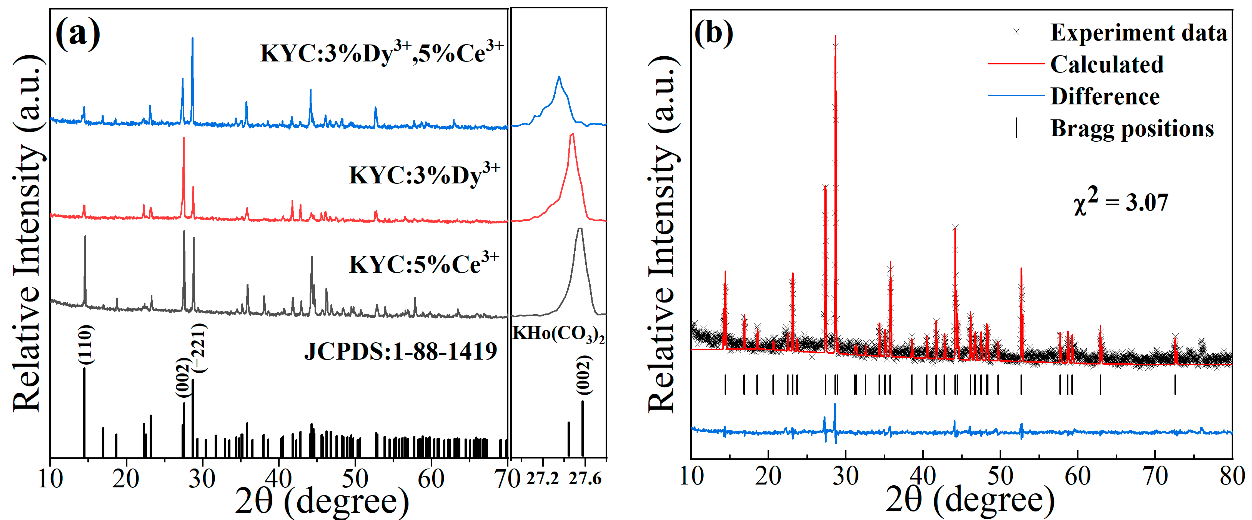


**Figure 1.** (a) XRD patterns of KYC:5%Ce<sup>3+</sup>, KYC:3%Dy<sup>3+</sup>, and KYC:3%Dy<sup>3+</sup>,5%Ce<sup>3+</sup>; (b) Rietveld refinements of KYC:3%Dy<sup>3+</sup>,5%Ce<sup>3+</sup>.

**Table 1.** Refined parameters of KYC:3%Dy<sup>3+</sup>,5%Ce<sup>3+</sup>.

Parameter	KY(CO <sub>3</sub> ) <sub>2</sub> [24]	KYC:3%Dy <sup>3+</sup> ,5%Ce <sup>3+</sup> [This Work]
Crystal System	Monoclinic	Monoclinic
Space group	C2/c	C2/c
a (Å)	8.488	8.489
b (Å)	9.442	9.447
c (Å)	6.913	6.922
α (°)	90.00	90.00
β (°)	110.963	110.94
γ (°)	90.00	90.00
Cell Volume (Å <sup>3</sup> )	517.4	518.340

### 3.2. Morphologies and Element Analysis

The morphologies of KYC:3%Dy<sup>3+</sup>,*y*%Ce<sup>3+</sup> (*y* = 0, 1, 2, 3, 4, 5, 6, 7) are illustrated in Figure 2a–h. According to the scanning electron microscopy images, both KYC hosts doped with Dy<sup>3+</sup> and Ce<sup>3+</sup> are monoclinic and consist of well-crystallized grains. In Figure 2a, for KYC:3%Dy<sup>3+</sup>, the grain size is relatively uniform, ranging from 20 to 50 microns. However, when Ce<sup>3+</sup> ions were added to KYC:3%Dy<sup>3+</sup>, the grains grew and became more likely to fracture. Many small particle fragments were found in the middle of the grains (Figure 2b–h). This fragmentation of grains may be caused by excessive internal stress in the grains due to the significant difference in ionic radii between Dy<sup>3+</sup> and Ce<sup>3+</sup>. Ce<sup>3+</sup> and Dy<sup>3+</sup> ions were doped into KYC through a chemical reaction that generates different small crystal nuclei for Ce<sup>3+</sup>, Dy<sup>3+</sup>, and Y<sup>3+</sup>. The crystals merge and grow, but due to differences in crystal growth direction between the various small crystal nuclei, it is impossible for the crystals to form a uniform size completely. As the concentration of Ce<sup>3+</sup> doping increases, primary grains that have not been completely merged can still be found at the fracture of bulk grains. The presence of pores and spaces between grains makes them more prone to fragmentation.

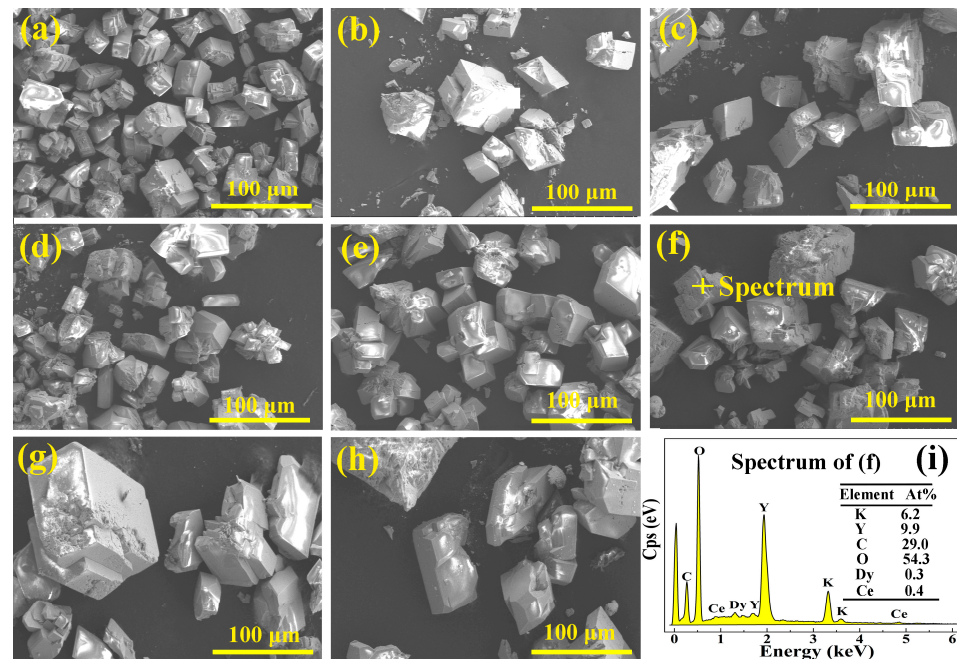


**Figure 2.** (a–h) Morphologies of KYC:3%Dy<sup>3+</sup>, y%Ce<sup>3+</sup> (y = 0, 1, 2, 3, 4, 5, 6, 7); (i) energy dispersive spectrum.

In addition, Figure 2i shows the elemental analysis of KYC:3%Dy<sup>3+</sup>, 5%Ce<sup>3+</sup> examined by energy dispersive spectroscopy. Although the doping concentrations of Ce<sup>3+</sup> and Dy<sup>3+</sup> are relatively low, it can still be observed from the energy spectrum that the grain contains elements such as K, Y, Ce, and Dy. The element contents of Y, Ce, and Dy are 9.9%, 0.4% and 0.3%, respectively. The ratio of Y to the total content of Ce and Dy is 14.1, which is close to the original stoichiometric ratio of 13.3. These results indicate that Ce<sup>3+</sup> and Dy<sup>3+</sup> have been successfully doped into the KYC host.

### 3.3. Luminescent Properties

Figure 3a displays the typical emission spectra of KYC:x%Dy<sup>3+</sup> when exposed to an excitation wavelength of 365 nm. The emission spectrum of Dy<sup>3+</sup> has four distinct emission bands, with peak values located at 492, 577, 666, and 756 nm. These peaks correspond to the transition from <sup>4</sup>F<sub>9/2</sub> to <sup>6</sup>H<sub>15/2</sub>, <sup>6</sup>H<sub>13/2</sub>, <sup>6</sup>H<sub>11/2</sub>, and <sup>6</sup>H<sub>9/2</sub> [14,28], respectively. The emission intensity initially increases and then decreases with the doping concentration of Dy<sup>3+</sup>. The maximum emission intensity occurs at a doping concentration of 3% Dy<sup>3+</sup>; excessive Dy<sup>3+</sup> ions will reduce the distance between two adjacent Dy<sup>3+</sup> ions, resulting in concentration quenching [16–18]. The reason is that cross-relaxation consumes the number of excited state electrons at the emission level of <sup>4</sup>F<sub>9/2</sub> between the two similar energy gaps of <sup>4</sup>F<sub>9/2</sub>–<sup>6</sup>F<sub>3/2</sub> and <sup>6</sup>H<sub>9/2</sub>–<sup>6</sup>H<sub>15/2</sub>. This relaxation process can be expressed as follows: <sup>4</sup>F<sub>9/2</sub>+<sup>6</sup>H<sub>15/2</sub> → <sup>6</sup>F<sub>3/2</sub>+<sup>6</sup>H<sub>9/2</sub>. Additionally, the emission of excited-state electrons in Dy<sup>3+</sup> mainly concentrates in the regions 462–504 nm and 553–597 nm. The emission colors are blue and yellow for the two main emission bands. To investigate the emission intensity, the emission intensities in the blue and yellow regions are integrated, and the relative intensities of the two emission bands are shown in Figure 3b. The ratios of blue-to-yellow light change with concentration and can be fitted linearly. The fitting results show that the integrated intensity ratio of blue and yellow light is close to 1, and the slope of the fitted line approaches 0. In the Dy<sup>3+</sup> emission spectrum, the emission of each spectral component remains stable, and the change in doping concentration does not induce hypersensitive transitions of the <sup>4</sup>F<sub>9/2</sub> → <sup>6</sup>H<sub>13/2</sub> [29]. The normal emission of yellow light indicates that Dy<sup>3+</sup> is in a relatively stable crystal field environment. The [DyO<sub>8</sub>] polyhedra in the KYC:Dy<sup>3+</sup> lattice effectively weaken the influence of external electric fields on Dy<sup>3+</sup> [24].

The energy transfers of adjacent  $\text{Dy}^{3+}$  between different polyhedra only occur through the zig-zag chains along the C-axis direction [25], which means that  $\text{Dy}^{3+}$  is less affected by the other electric field environment. Hence, the emission of electronic transitions between different energy levels is relatively stable.  $\text{Dy}^{3+}$  ions with different concentrations emit a single luminescent color. The luminescent properties of  $\text{Dy}^{3+}$  ions can be used for color modulation, especially for solid-state lighting. Multi-color luminescence can be achieved simply through spectral adjustment. Finally, 3% of  $\text{Dy}^{3+}$  was used to synthesize white light in the KYC host.

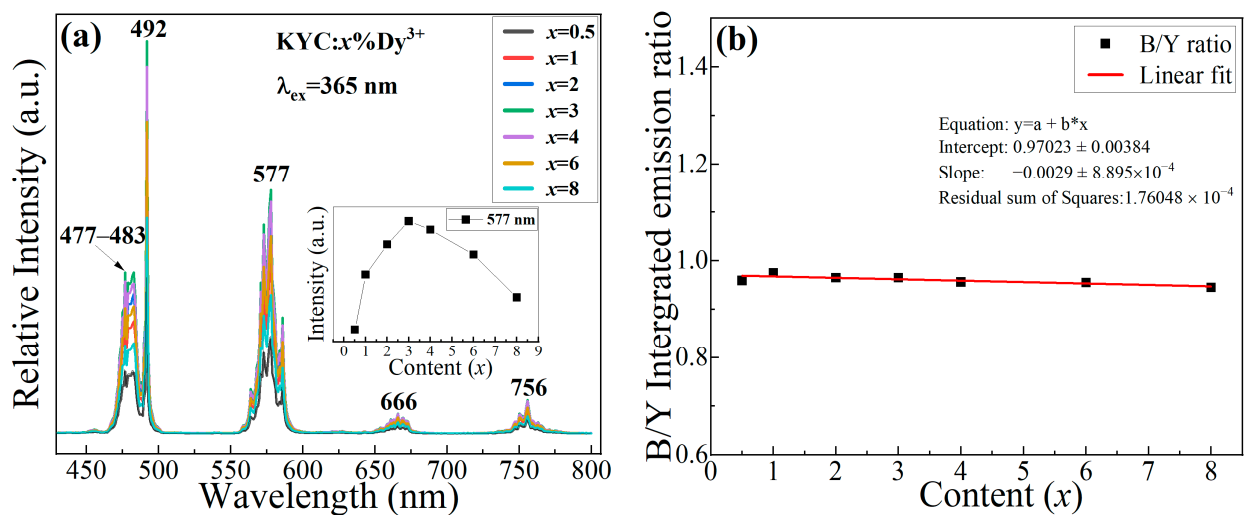


**Figure 3.** (a) Emission spectra of  $\text{Dy}^{3+}$ -doped KYC; (b) integrated intensity ratio of blue to yellow (B/Y).

Figure 4 clearly displays the excitation spectra of KYC doped with  $\text{Ce}^{3+}$  and  $\text{Dy}^{3+}$  monitored at 577 nm. Sharp excitation peaks are visible in the excitation spectrum of  $\text{KYC:3\%Dy}^{3+}$ . These peaks are observed at 325, 339, 351, 365, 386, 428, 453, and 476 nm and correspond to the transition of  $\text{Dy}^{3+}$  from  ${}^6\text{H}_{15/2}$  to  ${}^6\text{P}_{3/2}$ ,  ${}^4\text{I}_{9/2}$ ,  ${}^6\text{P}_{7/2}$ ,  ${}^6\text{P}_{5/2}$ ,  ${}^4\text{I}_{13/2}$ ,  ${}^4\text{G}_{11/2}$ ,  ${}^4\text{I}_{15/2}$ , and  ${}^4\text{F}_{9/2}$  [5,28], respectively. When  $\text{Ce}^{3+}$  was added to  $\text{KYC:3\%Dy}^{3+}$ , two broad absorption peaks were detected at 274 and 340 nm (monitoring at 577 nm), which belong to the energy transition of  $\text{Ce}^{3+}$  from 4f to 5d [30]. The excitation intensity of  $\text{KYC:3\%Dy}^{3+}, 5\%\text{Ce}^{3+}$  in the range of 230–360 nm is significantly greater than that of  $\text{KYC:3\%Dy}^{3+}$ . This is primarily due to the overlap of energy levels between  $\text{Ce}^{3+}$  and  $\text{Dy}^{3+}$ , which promotes electron resonance migration [31,32]. The other excitation intensities of  $\text{Dy}^{3+}$  at 428, 453, and 476 nm remain the same as before. Therefore, a higher excitation intensity benefits the emission of  $\text{Dy}^{3+}$  ions in the resonance excitation wavelength.

Figure 5 presents the emission spectra of  $\text{KYC:3\%Dy}^{3+}, y\%\text{Ce}^{3+}$ . In Figure 5a, the emission spectrum is mainly composed of the emission of  $\text{Ce}^{3+}$  and  $\text{Dy}^{3+}$ . The emission wavelength of  $\text{Ce}^{3+}$  is distributed in the range of 350–460 nm, while  $\text{Dy}^{3+}$  is in the range of 460–800 nm. When  $\text{KYC:3\%Dy}^{3+}, y\%\text{Ce}^{3+}$  is excited at 339 nm, the collaboration between  $\text{Ce}^{3+}$  and  $\text{Dy}^{3+}$  enables it to emit a higher fluorescence intensity. As shown in the figure, the emission intensity of  $\text{Ce}^{3+}$  is maximum when the  $\text{Ce}^{3+}$  concentration in  $\text{KYC:3\%Dy}^{3+}, y\%\text{Ce}^{3+}$  is 4, while the maximum emission intensity of  $\text{Dy}^{3+}$  corresponds to a  $\text{Ce}^{3+}$  concentration of 5. Before a concentration of 5%,  $\text{Ce}^{3+}$  ions enhance the emission intensity of  $\text{Dy}^{3+}$ . However, as the  $\text{Ce}^{3+}$  ion content continues to increase, the concentration quenching of  $\text{Ce}^{3+}$  weakens the emission intensity of  $\text{Dy}^{3+}$  [33]. This phenomenon is mainly caused by the electric multipole interaction between  $\text{Ce}^{3+}$  ions. The type of electric multipole interaction can be determined using Dexter's formula [34]:

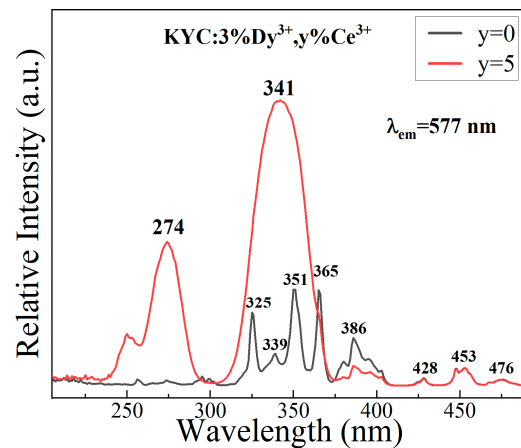


Figure 4. Excitation spectra of KYC:3%Dy<sup>3+</sup>,y%Ce<sup>3+</sup> ( $y = 0, 5$ ).

$$\frac{I}{\chi} = K[1 + \beta(\chi)^{\frac{\theta}{3}}]^{-1}$$

where  $I$  is the emission intensity of Ce<sup>3+</sup> at 399 nm,  $\chi$  is an activator concentration of Ce<sup>3+</sup> in KYC:Dy<sup>3+</sup>, Ce<sup>3+</sup>,  $\theta$  is a multipole–multipole interaction type, and  $K$  and  $\beta$  are constants. To obtain the value of  $\theta$ , the above equation can be simplified as follows:

$$\log \frac{I}{\chi} = -\frac{\theta}{3} \log \chi + C$$

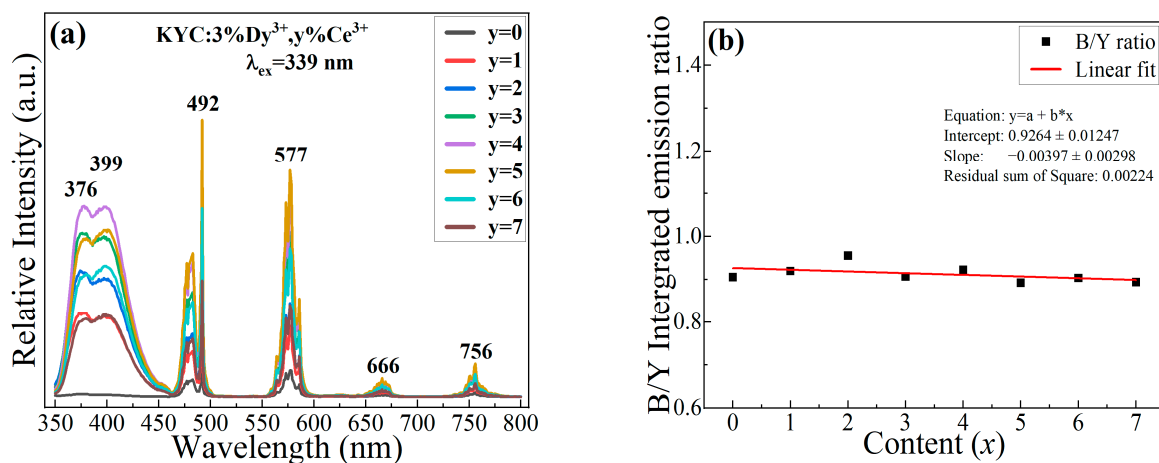
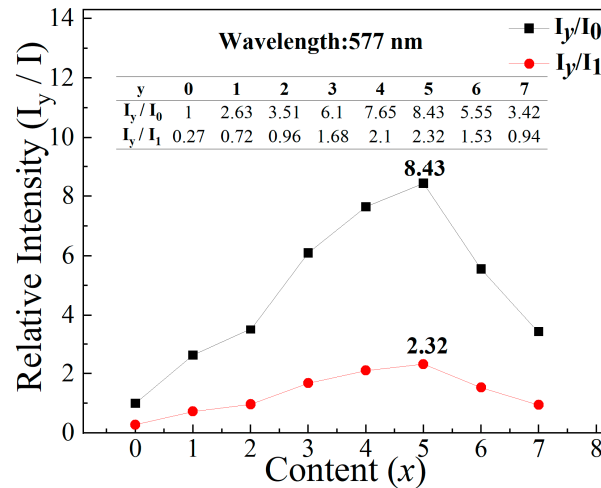


Figure 5. (a) Emission spectra of KYC:3%Dy<sup>3+</sup>,y%Ce<sup>3+</sup>; (b) integrated intensity ratio of blue to yellow (B/Y).

After fitting the Ce<sup>3+</sup> emission data, it was found that the value of  $\theta$  is close to 8. The result shows that the mechanism of Ce<sup>3+</sup> concentration quenching is attributed to the dipole–quadrupole.

The emission intensities of Dy<sup>3+</sup> in the presence of Ce<sup>3+</sup> ions were calculated in Figure 5b. The integral intensity ratios of blue to yellow are similar in KYC:3%Dy<sup>3+</sup>,y%Ce<sup>3+</sup> ( $y = 0-7$ ). The intensity ratio of each sample can be linearly fitted, and the slope of the fitted line is close to 0. The similar intensity ratio of Dy<sup>3+</sup> indicates that its emission has relative independence. The doping of Ce<sup>3+</sup> ions only enhances the emission of Dy<sup>3+</sup> through energy transfer and does not trigger the hypersensitive transition. The relative intensities at different  $y$  concentrations are shown in Figure 6. The enhancement values are described by  $I_y/I_0$  and  $I_y/I_1$  at the emission wavelength of 577 nm, where  $I_y$  and  $I_0$  are

the peak intensities excited by 339 nm at KYC:3%Dy<sup>3+</sup>,*y*%Ce<sup>3+</sup>, and KYC:3%Dy<sup>3+</sup>,0Ce<sup>3+</sup>,  $I_1$  is the maximum peak intensity excited by 365 nm in KYC:3%Dy<sup>3+</sup>. From the curves, the maximum value of enhancement occurs at a Ce<sup>3+</sup> concentration of 5%, which is 8.43 and 2.32 times for  $I_0$  and  $I_1$ , respectively. Therefore, Ce<sup>3+</sup> is employed to not only increase the emission intensity of Dy<sup>3+</sup> but also to adjust spectral components.



**Figure 6.** Relative intensities of KYC:3%Dy<sup>3+</sup>,*y*%Ce<sup>3+</sup> at different *y* concentrations.

### 3.4. Decay Curves

Figure 7 illustrates the typical photoluminescence decay curve of KYC:3%Dy<sup>3+</sup>,5%Ce<sup>3+</sup>. The phosphor was excited at 339 nm and emitted at 577 nm. From the figure, the decay curve can be fitted by a double-exponential function. The fitted residuals are well distributed around 0. The double-exponential fitting curve indicates that two main factors are dominating the radiation process of Dy<sup>3+</sup>. In general, the lifetimes vary with different concentrations due to the energy transfer between the Dy<sup>3+</sup> ions [35]. Therefore, a constant concentration of Dy<sup>3+</sup> was used to investigate the contribution of Ce<sup>3+</sup>. The lifetimes of Dy<sup>3+</sup> with different Ce<sup>3+</sup> concentrations (1% to 7%) were calculated. Table 2 provides the detailed values of lifetime for  $\tau_1$  and  $\tau_2$  corresponding to the double-exponential components. From the table, it can be observed that the  $\tau_1$  and  $\tau_2$  values increase with the increase in the Ce<sup>3+</sup> concentration in the range of 1% to 5%, which is consistent with the trend of emission intensity variation. The increase in lifetime is mainly attributed to the transfer of excited state electrons from Ce<sup>3+</sup> to Dy<sup>3+</sup>. Overlapping excitation bands are more prone to resonance transfer and cross-relaxation [14,31]. However, as the concentration of Ce<sup>3+</sup> continues to increase, the number of excited electrons in Dy<sup>3+</sup> decreases due to the quenching of the Ce<sup>3+</sup> concentration [33]. As a result, the lifetimes of Dy<sup>3+</sup> slightly decrease.

**Table 2.** Lifetimes of KYC:3%Dy<sup>3+</sup>,*y*%Ce<sup>3+</sup>.

No.	<i>y</i> %	$\tau_1$ ( $\mu$ s)	$\tau_2$ ( $\mu$ s)	$\tau$ ( $\mu$ s)
1	1%	274.3	949.1	826.1
2	2%	277.4	950.2	827.4
3	3%	290.1	974.7	844.5
4	4%	300.2	985.6	859.2
5	5%	308.4	993.3	858.7
6	6%	292.9	974.4	851.0
7	7%	311.5	985.9	850.7

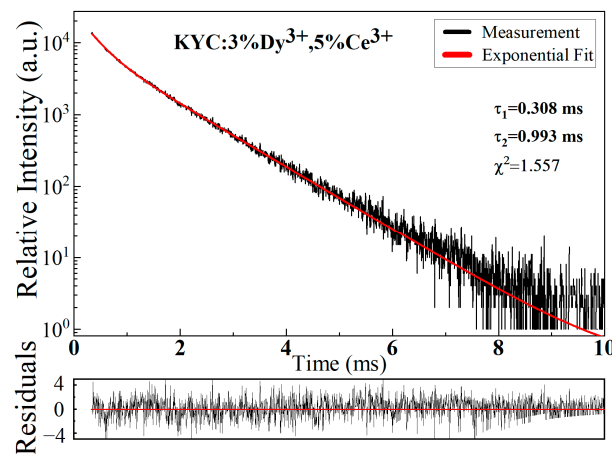


**Figure 7.** Photoluminescence decay curve of KYC: 3%Dy<sup>3+</sup>,5%Ce<sup>3+</sup>.

### 3.5. Energy Level Diagram

Figure 8 shows the energy transfer mechanism of KYC:Dy<sup>3+</sup>,Ce<sup>3+</sup>. When excited by 339 nm, the electrons of both Ce<sup>3+</sup> and Dy<sup>3+</sup> are stimulated from the ground state to the excited state simultaneously. In the Ce<sup>3+</sup> excited state of <sup>5</sup>D<sub>3/2</sub>, one of the electrons relaxes to <sup>2</sup>F<sub>5/2</sub> and <sup>2</sup>F<sub>7/2</sub> producing the emission of 375 and 396 nm through the lowest 5d excited state [31]. The other excited state electrons of Ce<sup>3+</sup> (<sup>5</sup>D<sub>3/2</sub>) could transfer to the excited energy level of Dy<sup>3+</sup> (<sup>4</sup>I<sub>9/2</sub>) by the resonance energy transfer (RET) [14,31]. For the excited state of Dy<sup>3+</sup>, the excited electrons initially relax to the lower excited state of <sup>4</sup>F<sub>9/2</sub> by non-radiation and then emit blue (<sup>6</sup>H<sub>15/2</sub>), yellow (<sup>6</sup>H<sub>13/2</sub>), and red (<sup>6</sup>H<sub>11/2</sub>, <sup>6</sup>H<sub>9/2</sub>) light when returning to the ground state [36]. This simultaneous excitation of Ce<sup>3+</sup> at 339 nm enhances the emission intensity of Dy<sup>3+</sup>. In addition, according to the emission spectra of KYC:3%Dy<sup>3+</sup>,4%Ce<sup>3+</sup> and KYC:3%Dy<sup>3+</sup>,5%Ce<sup>3+</sup>, there were no simultaneous increases or decreases in the emission intensity of Ce<sup>3+</sup> and Dy<sup>3+</sup> ions, indicating the existence of other energy transfer forms. The energy levels of <sup>6</sup>P<sub>5/2</sub> (Dy<sup>3+</sup>) and <sup>4</sup>K<sub>17/2</sub> (Dy<sup>3+</sup>) in an excited state are 27,503 and 26,365 cm<sup>-1</sup> [37]. Due to the overlap of Ce<sup>3+</sup> emission and Dy<sup>3+</sup> excitation, the energy of the Ce<sup>3+</sup> excited state electrons can be transported from Ce<sup>3+</sup> to Dy<sup>3+</sup> by the cross-relaxation (CR). The cross-relaxation processes can be described as <sup>5</sup>D<sub>3/2</sub>+<sup>6</sup>H<sub>15/2</sub> → <sup>2</sup>F<sub>5/2</sub>+<sup>6</sup>P<sub>5/2</sub> and <sup>5</sup>D<sub>3/2</sub>+<sup>6</sup>H<sub>15/2</sub> → <sup>2</sup>F<sub>7/2</sub>+<sup>4</sup>K<sub>17/2</sub>. When the concentration of Ce<sup>3+</sup> exceeds 5%, the emission intensities of Ce<sup>3+</sup> and Dy<sup>3+</sup> decrease simultaneously due to the concentration quenching of Ce<sup>3+</sup>.

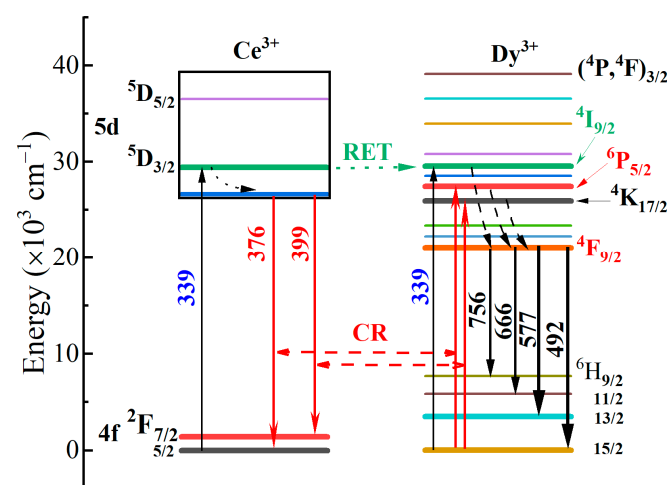


**Figure 8.** Energy transfer mechanism of Ce<sup>3+</sup> and Dy<sup>3+</sup> in KYC:3%Dy<sup>3+</sup>,y%Ce<sup>3+</sup>.

### 3.6. Chromaticity Coordinates

The  $\text{Dy}^{3+}$  emission spectrum comprises blue, yellow, and red components. In the  $\text{KYC:3\%Dy}^{3+},y\%\text{Ce}^{3+}$  spectrum, the emission intensity of yellow light is consistently similar to that of blue light at different  $\text{Ce}^{3+}$  concentrations. Therefore, the luminescence color can be adjusted by changing the concentration of  $\text{Ce}^{3+}$  ions. Figure 9 shows the chromaticity coordinates of  $\text{KYC:3\%Dy}^{3+},y\%\text{Ce}^{3+}$  ( $y = 0-7$ ) and  $\text{KYC:5\%Ce}^{3+}$ . From the graph, it is evident that  $\text{KYC:3\%Dy}^{3+}$  emits light in the yellow-green region,  $\text{KYC:5\%Ce}^{3+}$  emits light in the purplish-blue region, and all Ce-doped  $\text{KYC:3\%Dy}^{3+},y\%\text{Ce}^{3+}$  ( $y = 1-7$ ) color coordinates appear in the white light region. The  $\text{KYC:Dy}^{3+}$  phosphor is used for white light mainly due to the relatively consistent and high emission intensity of blue and yellow light in the  $\text{Dy}^{3+}$  emission spectrum. Moreover,  $\text{KYC:Dy}^{3+}$  luminescent color is close to daylight, and its luminescent color is similar to the emission of  $\text{Dy}^{3+}$  in  $\text{Bi}(\text{PO}_4)_6$  [3],  $\text{Y}_4\text{Al}_2\text{O}_5$  [5], and  $\text{K}_3\text{YB}_6\text{O}_{12}$  [16], belonging to warm white light. It is easy to adjust the luminescent color by adding other luminescent ions to the  $\text{KYC:Dy}^{3+}$ , while the luminescent color of  $\text{Dy}^{3+}$  remains constant.

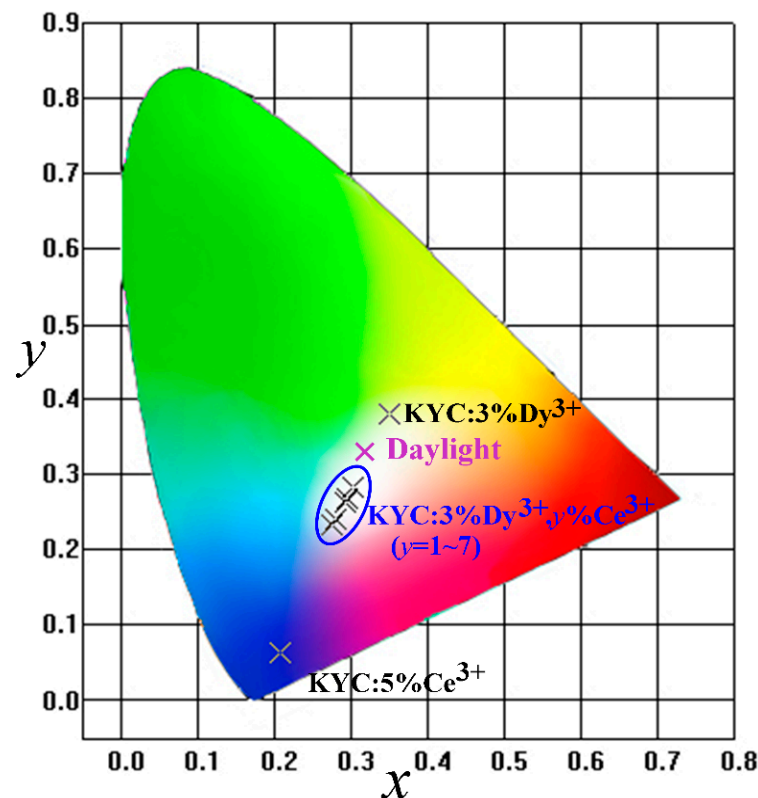


Figure 9. CIE chromaticity coordinates ( $\times$ ) of  $\text{KYC: 3\%Dy}^{3+},y\%\text{Ce}^{3+}$  excited at 339 nm.

The correlated color temperatures were calculated by the formula [38], and the detailed values are provided in Table 3. The coordinate of  $\text{KYC:3\%Dy}^{3+},5\%\text{Ce}^{3+}$  is (0.3204, 0.2972) with a correlated color temperature of 6270 K, which is closer to standard daylight (0.33, 0.33). Moreover, the other Ce-doped KYCs emit cold white light. These cold white lights have relatively high color temperatures and can be used in locations that require clear vision, such as factories, exhibition rooms, conference rooms, or product exhibitions.

**Table 3.** Chromaticity coordinates and correlated color temperatures.

NO.	Samples	x	y	CCT (K)
1	KYC: 3%Dy <sup>3+</sup>	0.3517	0.3524	4762
2	KYC: 3%Dy <sup>3+</sup> ,1%Ce <sup>3+</sup>	0.3038	0.2743	8067
3	KYC:3%Dy <sup>3+</sup> ,2%Ce <sup>3+</sup>	0.3034	0.2737	8129
4	KYC: 3%Dy <sup>3+</sup> ,3%Ce <sup>3+</sup>	0.3174	0.2919	6527
5	KYC: 3%Dy <sup>3+</sup> ,4%Ce <sup>3+</sup>	0.3138	0.2860	6879
6	KYC:3%Dy <sup>3+</sup> ,5%Ce <sup>3+</sup>	0.3204	0.2972	6270
7	KYC: 3%Dy <sup>3+</sup> ,6%Ce <sup>3+</sup>	0.3149	0.2869	6777
8	KYC: 3%Dy <sup>3+</sup> ,7%Ce <sup>3+</sup>	0.3129	0.2840	6984
9	KYC: 5%Ce <sup>3+</sup>	0.2078	0.0632	1759
10	Daylight	0.33	0.33	5616

#### 4. Conclusions

Monoclinic KYC:Dy<sup>3+</sup>,Ce<sup>3+</sup> was successfully prepared by the hydrothermal method. In the KYC host, Dy<sup>3+</sup> maintains relatively independent emission characteristics. The relative intensity of blue and yellow light in the emission spectrum is not affected by the doping concentration of Dy<sup>3+</sup> ions. Even when Ce<sup>3+</sup> and Dy<sup>3+</sup> are co-doped with KYC, Dy<sup>3+</sup> can still maintain relatively independent emission. The relative intensity ratio of blue-to-yellow light is a constant value in each sample. The cross-relaxation and resonance energy transfer between Ce<sup>3+</sup> and Dy<sup>3+</sup> effectively enhance the emission intensity of Dy<sup>3+</sup>. Moreover, all Ce-doped KYC samples can emit white light. The light emitted by KYC:3%Dy<sup>3+</sup>,5%Ce<sup>3+</sup> is closest to standard daylight. These results indicate that both Ce<sup>3+</sup> and Dy<sup>3+</sup> ions maintain relatively independent emission characteristics in the KYC host, which makes it convenient to tune the emission color.

**Author Contributions:** Conceptualization, D.L. and L.H.; methodology, L.H., S.S. and J.Q.; validation, D.L. and L.H.; formal analysis, D.L. and L.H.; investigation, D.L.; resources, L.H.; data curation, L.H., S.S. and J.Q.; writing—original draft preparation, L.H.; writing—review and editing, D.L.; visualization, D.L.; supervision, D.L.; project administration, D.L.; and funding acquisition, D.L. All authors have read and agreed to the published version of the manuscript.

**Funding:** This research was funded by the University Natural Science Research Project of Anhui Province, grant numbers 2023AH050311, 2023AH010043, and 2023AH010044.

**Institutional Review Board Statement:** Not applicable.

**Informed Consent Statement:** Not applicable.

**Data Availability Statement:** Data are contained within the article.

**Conflicts of Interest:** The authors declare no conflicts of interest.

#### References

- Chandrappa, V.; Basavapoornima, C.; Venkatramu, V.; Depuru, S.R.; Kaewkhao, J.; Pecharapa, W.; Jayasankar, C.K. A critical review and future prospects of Dy<sup>3+</sup>-doped glasses for white light emission applications. *Optik* **2022**, *266*, 169583. [CrossRef]
- Reddy, L. A Review of the Efficiency of White Light (or Other) Emissions in Singly and Co-Doped Dy<sup>3+</sup> Ions in Different Host (Phosphate, Silicate, Aluminate) Materials. *J. Fluoresc.* **2023**, *33*, 2181–2192. [CrossRef]
- Nandanwar, C.M.; Kokode, N.S.; Yerpude, A.N.; Dhoble, S.J. Luminescence properties of BiPO<sub>4</sub>:Ln (Ln = Dy<sup>3+</sup>, Tb<sup>3+</sup> and Sm<sup>3+</sup>) orthophosphate phosphors for near-UV-based solid-state lighting. *Bull. Mater. Sci.* **2023**, *46*, 51. [CrossRef]
- Alqarni, A.S.; Bulus, I.; Yusof, N.N.; Alomar, M.; Ghoshal, S.K. Luminescence properties of Dy<sup>3+</sup> doped B<sub>2</sub>O<sub>3</sub>-CaMg(CO<sub>3</sub>)<sub>2</sub>-TeO<sub>2</sub> glasses: A promising host for solid state lighting devices. *Opt. Laser Technol.* **2024**, *170*, 110327. [CrossRef]
- Kumar, P.; Singh, D.; Gupta, I.; Singh, S.; Nehra, S.; Kumar, R. A study of phase evolution, crystallographic and down-conversion luminescent behaviour of monoclinic Y<sub>4</sub>Al<sub>2</sub>O<sub>9</sub>:Dy<sup>3+</sup> nanophosphors for white light applications. *Opt. Mater.* **2023**, *138*, 113677. [CrossRef]
- Bindhu, A.; Naseemabeevi, J.I.; Ganesanpotti, S. Insights into the crystal structure and photophysical response of Dy<sup>3+</sup> doped Li<sub>3</sub>Y<sub>3</sub>Te<sub>2</sub>O<sub>12</sub> for ratiometric temperature sensing. *J. Sci. Adv. Mater. Dev.* **2022**, *7*, 100444. [CrossRef]
- Vu, T.H.Q.; Stefańska, D.; Dereń, P.J. Effect of A-Cation Radius on the Structure, Luminescence, and Temperature Sensing of Double Perovskites A<sub>2</sub>MgWO<sub>6</sub> Doped with Dy<sup>3+</sup> (A = Ca, Sr, Ba). *Inorg. Chem.* **2023**, *62*, 20020–20029. [CrossRef]

8. Abbas, M.T.; Khan, S.A.; Mao, J.; Khan, N.Z.; Qiu, L.; Ahmed, J.; Wei, X.; Chen, Y.; Alshehri, S.M.; Agathopoulos, S. Optical thermometry based on the luminescence intensity ratio of Dy<sup>3+</sup>-doped GdPO<sub>4</sub> phosphors. *J. Therm. Anal. Calorim.* **2022**, *147*, 11769–11775. [[CrossRef](#)]
9. Vidya Saraswathi, A.; Prabhu, N.S.; Naregundi, K.; Sayyed, M.I.; Murari, M.S.; Almuqrin, A.H.; Kamath, S.D. Thermoluminescence investigations of Ca<sub>2</sub>Al<sub>2</sub>SiO<sub>7</sub>:Dy<sup>3+</sup> phosphor for gamma dosimetry applications. *Mater. Chem. Phys.* **2022**, *281*, 125872. [[CrossRef](#)]
10. Shashikala, B.S.; Premkumar, H.B.; Sharma, S.C.; Nagabhushana, H.; Daruka Prasad, B.; Darshan, G.P. Dy<sup>3+</sup> ions activated CaAl<sub>2</sub>O<sub>4</sub> nanophosphors: Photoluminescent and photometric properties prompted manifold applications. *Inorg. Chem. Commun.* **2022**, *142*, 109619. [[CrossRef](#)]
11. Jung, J.-y.; Kim, J.; Shim, Y.-S.; Hwang, D.; Son, C.S. Structure and Photoluminescence Properties of Rare-Earth (Dy<sup>3+</sup>, Tb<sup>3+</sup>, Sm<sup>3+</sup>)-Doped BaWO<sub>4</sub> Phosphors Synthesized via Co-Precipitation for Anti-Counterfeiting. *Materials* **2020**, *13*, 4165. [[CrossRef](#)]
12. İlhan, M.; Keskin, İ.Ç.; Gültekin, S. Assessing of Photoluminescence and Thermoluminescence Properties of Dy<sup>3+</sup> Doped White Light Emitter TTB-Lead Metatantalate Phosphor. *J. Electron. Mater.* **2020**, *49*, 2436–2449. [[CrossRef](#)]
13. Luewarasirikul, N.; Kaewkhao, J. Light-emitting CaMoO<sub>4</sub>:Dy<sup>3+</sup> phosphors for photonic materials: Synthesis and luminescence properties. *AIP Conf. Proc.* **2020**, *2279*, 060009.
14. Lodi, T.A.; Dantas, N.F.; Gonçalves, T.S.; de Camargo, A.S.S.; Pedrochi, F.; Steimacher, A. Dy<sup>3+</sup> doped calcium boroaluminate glasses and Blue Led for smart white light generation. *J. Lumin.* **2019**, *207*, 378–385. [[CrossRef](#)]
15. Chidthong, R.; Insiripong, S.; Angnanon, A.; Tipwan, J.; Rajaramakrishna, R.; Kaewkhao, J. Photoluminescence properties of Bi<sub>2</sub>MoO<sub>6</sub>:Dy<sup>3+</sup> phosphors fabricated by solid state reactions. *AIP Conf. Proc.* **2020**, *2279*, 060007.
16. Fu, Y.; Zhang, Z.; Zhang, F.; Li, C.; Liu, B.; Li, G. Electronic structure, energy transfer mechanism and thermal quenching behavior of K<sub>3</sub>YB<sub>6</sub>O<sub>12</sub>:Dy<sup>3+</sup>, Eu<sup>3+</sup> phosphor. *Opt. Mater.* **2020**, *99*, 109519. [[CrossRef](#)]
17. Meena, M.L.; Som, S.; Singh, R.K.; Lu, C.-H. Synthesis, spectroscopic characterization and estimation of Judd-Ofelt parameters for Dy<sup>3+</sup> activated Li<sub>2</sub>MgZrO<sub>4</sub> double perovskite materials. *Polyhedron* **2020**, *177*, 114322. [[CrossRef](#)]
18. Sehrawat, P.; Khatkar, A.; Boora, P.; Kumar, M.; Singh, S.; Malik, R.K.; Khatkar, S.P.; Taxak, V.B. Fabrication of single-phase BaLaAlO<sub>4</sub>:Dy<sup>3+</sup> nanophosphors by combustion synthesis. *Mater. Manuf. Process.* **2020**, *35*, 1259–1267. [[CrossRef](#)]
19. Kaewnuam, E.; Wantana, N.; Kim, H.J.; Kaewkhao, J. Study on structure and luminescence properties of LaBMoO<sub>6</sub>:Dy<sup>3+</sup> phosphor for photonic material applications. *J. Meta Mater. Min.* **2018**, *28*, 63–68.
20. Gupta, S.K.; Jafar, M.; Thekke Parayil, R.; Bahadur, J.; Sudarshan, K. White light emitting nanocrystalline Y<sub>1-x</sub>Gd<sub>x</sub>PO<sub>4</sub>:Dy<sup>3+</sup> and improved PLQY on Gd<sup>3+</sup> co-doping. *Inorg. Chem. Commun.* **2024**, *159*, 111908. [[CrossRef](#)]
21. Girisha, H.R.; Krushna, B.R.R.; Prasad, B.D.; Sharma, S.C.; Srikanth, C.; Kumar, J.B.P.; Nagabhushana, H. A novel single phase La<sub>2</sub>CaZnO<sub>5</sub>:Dy<sup>3+</sup> phosphor for potential applications in WLED's, latent fingerprint and cheilioscopy. *J. Lumin.* **2023**, *255*, 119539. [[CrossRef](#)]
22. Cao, X.; Li, X.; Chen, X.; Xu, S.; Xiong, D.; Deng, W. Preparation, characterization and optical properties of Dy-doped yttrium aluminum garnet. *Int. J. Mod. Phys. B* **2017**, *31*, 1744071. [[CrossRef](#)]
23. Koseva, I.; Tzvetkov, P.; Ivanov, P.; Gancheva, M.; Nikolov, V. Dysprosium doped calcium germanate (Ca<sub>2</sub>GeO<sub>4</sub>) as a candidate for LED application. *J. Int. Sci. Publ. Mater. Methods Technol.* **2019**, *13*, 18–24.
24. Cao, L.; Peng, G.; Yan, T.; Luo, M.; Lin, C.; Ye, N. Three alkaline-rare earth cations carbonates with large birefringence in the deep UV range. *J. Alloys Compd.* **2018**, *742*, 587–593. [[CrossRef](#)]
25. Li, D.; Zhu, G. Quantum Cutting in Ultraviolet B-Excited KY(CO<sub>3</sub>)<sub>2</sub>:Tb<sup>3+</sup> Phosphors. *Materials* **2022**, *15*, 6160. [[CrossRef](#)] [[PubMed](#)]
26. Shannon, R. Revised effective ionic radii and systematic studies of interatomic distances in halides and chalcogenides. *Acta Crystallogr.* **1976**, *32*, 751–767. [[CrossRef](#)]
27. Kutlu, I.; Kalz, H.-J.; Wartchow, R.; Ehrhardt, H.; Seidel, H.; Meyer, G. Kalium-Lanthanoid-Carbonate, KM(CO<sub>3</sub>)<sub>2</sub> (M = Nd, Gd, Dy, Ho, Yb). *Z. Anorg. Allg. Chem.* **1997**, *623*, 1753–1758. [[CrossRef](#)]
28. Song, R.; Zhang, Z.; Li, H.; Luo, Z.; Yang, J.; Ma, J.; Xiang, X.; Zeng, Q.; Zhu, J. A single-phase white-emitting La(BO<sub>3</sub>,PO<sub>4</sub>):Dy<sup>3+</sup> phosphor with high thermostability. *Ceram. Int.* **2023**, *49*, 6965–6973. [[CrossRef](#)]
29. Kesavulu, C.R.; Kim, H.J.; Lee, S.W.; Kaewkhao, J.; Chanthima, N.; Tariwong, Y. Physical, vibrational, optical and luminescence investigations of Dy<sup>3+</sup>-doped yttrium calcium silicoborate glasses for cool white LED applications. *J. Alloys Compd.* **2017**, *726*, 1062–1071. [[CrossRef](#)]
30. Feng, J.; Yuan, S.; Wu, X.; Zhu, D.; Chen, J.; Mu, Z. KCaLa(PO<sub>4</sub>)<sub>2</sub>:Ce<sup>3+</sup>, Dy<sup>3+</sup> Phosphors for White Light-Emitting Diodes with Abnormal Thermal Quenching and High Quantum Efficiency. *J. Electron. Mater.* **2021**, *50*, 6283–6290. [[CrossRef](#)]
31. Cheng, Y.; Liu, S.; Zhu, D. Tunable emission, energy transfer and thermal stability of a single-phased Sr<sub>(1-x-y)</sub>MgP<sub>2</sub>O<sub>7</sub>:xCe<sup>3+</sup>, yDy<sup>3+</sup> phosphor for ultraviolet converted white LEDs. *J. Alloys Compd.* **2019**, *783*, 19–27.
32. Choubey, S.R.; Gedam, S.C.; Dhoble, S.J. Resonant and non-resonant energy transfer from Ce<sup>3+</sup> → X (X = Tb<sup>3+</sup>, Eu<sup>3+</sup> or Dy<sup>3+</sup>) in NaMgSO<sub>4</sub>F material. *Luminescence* **2017**, *32*, 253–256. [[CrossRef](#)]
33. Richhariya, T.; Brahme, N.; Bisen, D.P.; Badapanda, T.; Tiwari, K.; Jain, A. Investigation of photoluminescence, thermoluminescence, and energy transfer mechanism in Ce/Dy co-doped Sr<sub>2</sub>Al<sub>2</sub>SiO<sub>7</sub>. *Mater. Sci. Semicon. Proc.* **2023**, *159*, 107396. [[CrossRef](#)]

34. Hargunani, S.P.; Sonekar, R.P.; Singh, A.; Khosla, A.; Arya, S. Structural and spectral studies of Ce<sup>3+</sup> doped Sr<sub>3</sub>Y(BO<sub>3</sub>)<sub>3</sub> nano phosphors prepared by combustion synthesis. *Mater. Technol.* **2022**, *37*, 450–461. [[CrossRef](#)]
35. Karacaoglu, E. Synthesis and effects of co-dopants (La<sup>3+</sup>, Sm<sup>3+</sup>, Mn<sup>2+</sup>, Nd<sup>3+</sup>, V<sup>5+</sup>, Y<sup>3+</sup>) on photoluminescence of SrAl<sub>2</sub>O<sub>4</sub>:Dy<sup>3+</sup> phosphor. *Luminescence* **2022**, *37*, 1714–1724. [[CrossRef](#)] [[PubMed](#)]
36. Bandi, V.R.; Nien, Y.-T.; Chen, I.-G. Enhancement of white light emission from novel Ca<sub>3</sub>Y<sub>2</sub>Si<sub>3</sub>O<sub>12</sub>:Dy<sup>3+</sup> phosphors with Ce<sup>3+</sup> ion codoping. *J. Appl. Phys.* **2010**, *108*, 023111. [[CrossRef](#)]
37. Carnall, W.T.; Fields, P.R.; Rajnak, K. Electronic Energy Levels in the Trivalent Lanthanide Aquo Ions. I. Pr<sup>3+</sup>, Nd<sup>3+</sup>, Pm<sup>3+</sup>, Sm<sup>3+</sup>, Dy<sup>3+</sup>, Ho<sup>3+</sup>, Er<sup>3+</sup>, and Tm<sup>3+</sup>. *J. Chem. Phys.* **1968**, *49*, 4424–4442. [[CrossRef](#)]
38. Durmus, D. Correlated color temperature: Use and limitations. *Light. Res. Technol.* **2021**, *54*, 363–375. [[CrossRef](#)]

**Disclaimer/Publisher’s Note:** The statements, opinions and data contained in all publications are solely those of the individual author(s) and contributor(s) and not of MDPI and/or the editor(s). MDPI and/or the editor(s) disclaim responsibility for any injury to people or property resulting from any ideas, methods, instructions or products referred to in the content.